(Received 23 June 2026, Accepted 2 August 2026, Scheduled 20 August 2026)

Design and Implementation of a Triple-Band Bandstop Filter with Controllable Bandwidth and Stopband Rejection

Chuan Shao[1,*], Xin Gao[2], Baotong Gou[1], Rong Cai[1], Xinnai Zhang[1], and Kai Xu[3]

[1]*Nantong Key Laboratory of Artificial Intelligence New Quality Technology, Jiangsu College of Engineering and Technology Nantong Jiangsu 226000, China*
[2]*Shanghai Institute of Satellite Engineering, Shanghai 201109, China*
[3]*School of Information Science and Technology, Nantong University, Nantong, Jiangsu 226019, China*

ABSTRACT: In this article, a triple-band bandstop filter employing coupled tri-section stepped-impedance resonators is proposed. The characteristic impedances of individual stepped-impedance sections are judiciously adjusted to allocate the three stopband frequencies. Subsequently, the coupling coefficients between adjacent resonators are meticulously tuned to simultaneously regulate the bandwidth of each stopband and the corresponding suppression level within the rejection bands. Moreover, out-of-band insertion and return losses are optimized by properly selecting the characteristic impedance of half-wavelength transmission lines interconnecting resonators. To experimentally validate the aforementioned design methodology, a triple-band bandstop filter with stopband center frequencies of 1.2 GHz, 3 GHz, and 4.8 GHz is designed, simulated, fabricated, and measured. The measured responses are found in excellent agreement with simulated results, thereby conclusively substantiating the proposed design concept.

1. INTRODUCTION

Driven by the ever-increasing spectrum congestion and coexistence of multiple wireless communication standards, microwave bandstop filters with high suppression levels and multi-band operation capability have become indispensable for effectively rejecting unwanted signals, intermodulation distortions, and spurious responses within densely populated frequency spectra [1–3].

Generally, two fundamental approaches are employed realize bandstop filters. The first approach utilizes shunt series-resonant branches, which exhibit zero input impedance at the resonant frequency and thereby equivalently short-circuit the main transmission path to ground, consequently diverting the signal and creating the desired stopband. Alternatively, the second approach is based on series-parallel-resonant branches, which present infinite input impedance at resonance and thus equivalently open-circuit the transmission line, thereby blocking signal propagation and establishing rejection band [4].

Similarly, the design methodologies for multi-band bandstop filters are predominantly derived from and extended upon these two fundamental configurations [5–12]. Distinct from the conventional design methodology of single-band bandstop filters, the branches employed in multi-band configurations generally incorporate multi-mode resonators or multiple sets of resonators with distinct resonant frequencies, thereby correspondingly establishing the respective stopbands.

In [5], Hilbert-fork resonators have been employed to realize a triple-band bandstop filter using the shunt series-resonant topology. Bandstop filters based on this topology generally necessitate the fabrication of extremely narrow gaps; consequently, stringent fabrication tolerances are inevitably imposed. Subsequently, in [6–9], triple-band bandstop filters based on a series-parallel-resonant topology have been implemented by using triple-mode stepped-impedance resonators. Compared with the aforementioned approaches, this design methodology is considerably simpler and obviates the necessity for narrow gaps. Nevertheless, in the aforementioned designs, the matching of out-of-band passbands has not been taken into consideration, resulting in excessively large insertion losses within passband regions.

Likewise, based on the same series parallel-resonant branch topology, defected ground structures have been adopted in [10]. Although the out-of-band performance has been improved in this design, the employment of defected ground structures inherently restricts their applicability.

Furthermore, in [11], a triple-band bandstop filter has been synthesized by judiciously combining the aforementioned two topologies, and defected microstrip line structures together with half-wavelength microstrip resonators are concurrently used. This design offers considerable flexibility, and each stopband can be controlled and adjusted. Nevertheless, it may suffer from relatively large physical dimensions and rather complex design procedures. In [12], a dual-band bandstop filter employing tri-section stepped-impedance resonators has been demonstrated, and a wide upper passband is achieved through the deliberate cancellation of the first spurious mode.

In this paper, a triple-band bandstop filter with controllable bandwidth and stopband rejection is proposed. The proposed filter not only achieves favorable suppression levels and bandwidths within the stopbands, but also exhibits low insertion loss

* Corresponding author: Chuan Shao (ch_shao@jcet.edu.cn).

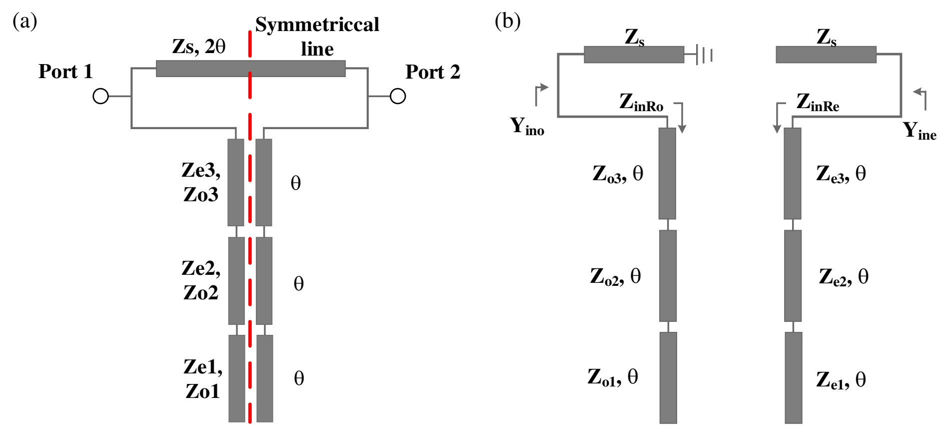

FIGURE 1. (a) Schematic diagram and (b) odd- and even-mode equivalent circuits of the developed triple-band bandstop filter.

and high return loss in the operating passbands. Consequently, the stopband rejection performance and out-of-band transmission characteristics are simultaneously guaranteed, thereby ensuring minimal signal degradation and excellent impedance matching across desired passband regions.

2. DESIGN AND ANALYSIS OF THE DEVELOPED TRIPLE-BAND BANDSTOP FILTER

2.1. Resonant Frequencies

The schematic diagram of the developed triple-band bandstop filter is given in Fig. 1(a). Since the proposed filter is structurally symmetric with respect to the symmetrical line, the even-odd mode analysis method can be employed [13]. Consequently, the corresponding odd- and even-mode equivalent circuits are derived by imposing electric and magnetic walls, respectively, along the symmetrical line, as illustrated in Fig. 1(b).

According to [13], Y_{ino} and Y_{ine} can be derived as:

$$Y_{\text{ino}} = -j\frac{\cot\theta}{Z_s} + \frac{1}{Z_{\text{inRo}}} \tag{1}$$

$$Z_{\text{inRo}} = jZ_{o3}\frac{(Z_{o3}Z_{o2}+Z_{o3}Z_{o1}+Z_{o2}^2)\tan^2\theta - Z_{o2}Z_{o1}}{-Z_{o2}^2\tan^3\theta+(Z_{o3}Z_{o2}+Z_{o3}Z_{o1}+Z_{o2}Z_{o1})\tan\theta} \tag{2}$$

$$Y_{\text{ine}} = j\frac{\tan\theta}{Z_s} + \frac{1}{Z_{\text{inRe}}} \tag{3}$$

$$Z_{\text{inRe}} = jZ_{e3}\frac{(Z_{e3}Z_{e2}+Z_{e3}Z_{e1}+Z_{e2}^2)\tan^2\theta - Z_{e2}Z_{e1}}{-Z_{e2}^2\tan^3\theta+(Z_{e3}Z_{e2}+Z_{e3}Z_{e1}+Z_{e2}Z_{e1})\tan\theta} \tag{4}$$

By imposing the condition $Y_{\text{ino}} = 0$, the following relation is derived:

$$\tan^2\theta = \frac{Z_sD+Z_{o3}A\pm\sqrt{(Z_sD+Z_{o3}A)^2s-4Z_sZ_{o3}Z_{o2}^3Z_{o1}}}{2Z_sZ_{o2}^2} \tag{5}$$

$$A = Z_{o3}Z_{o2}+Z_{o3}Z_{o1}+Z_{o2}^2,\ D = Z_{o3}Z_{o2}+Z_{o3}Z_{o1}+Z_{o2}Z_{o1} \tag{6}$$

From the above equations, it can be observed that the discriminant is greater than zero. Consequently, four resonant frequencies of the odd mode are obtained as follows:

$$\theta_{o1} = \arctan\sqrt{\frac{\left(\begin{array}{c}Z_sD+Z_{o3}A-\\ \sqrt{(Z_sD+Z_{o3}A)^2-4Z_sZ_{o3}Z_{o2}^3Z_{o1}}\end{array}\right)}{2Z_sZ_{o2}^2}} \tag{7a}$$

$$\theta_{o2} = \arctan\sqrt{\frac{\left(\begin{array}{c}Z_sD+Z_{o3}A+\\ \sqrt{(Z_sD+Z_{o3}A)^2-4Z_sZ_{o3}Z_{o2}^3Z_{o1}}\end{array}\right)}{2Z_sZ_{o2}^2}} \tag{7b}$$

$$\theta_{o3} = \pi - \theta_{o1} \tag{7c}$$

$$\theta_{o4} = \pi - \theta_{o2} \tag{7d}$$

Similarly, by setting $Y_{\text{ine}} = 0$, two resonant frequencies of the even mode are derived as:

$$\theta_{e1} = \arctan\sqrt{\frac{Z_s(Z_{e3}Z_{e2}+Z_{e3}Z_{e1}+Z_{e2}Z_{e1})+Z_{e3}Z_{e2}Z_{e1}}{Z_{e3}(Z_{e3}Z_{e2}+Z_{e3}Z_{e1}+Z_{e2}^2)+Z_sZ_{e2}^2}} \tag{8a}$$

$$\theta_{e2} = \pi - \theta_{e1} \tag{8b}$$

Specifically, it should be respectfully clarified that the purpose of imposing $Y_{\text{ino}} = 0$ or $Y_{\text{ine}} = 0$ in Eqs. (7a)–(8b) is not to precisely calculate the exact number and positions of transmission poles. Instead, these conditions are employed merely to identify and estimate the number of resonant modes (transmission poles) in the vicinity of stopbands. Accordingly, in this work, as in Fig. 2, the odd- and even-mode input admittances are set to zero solely for the purpose of determining the number of transmission poles, rather than for precisely locating their positions.

Therefore, within the frequency range from DC to $2f_0$, in addition to the two transmission poles located at DC and $2f_0$, a maximum of six transmission poles can be achieved by appropriately adjusting the characteristic impedance values of each section. As is well known, a greater number of transmission poles can enhance the roll-off characteristics at the edges of the stopband, thereby improving the overall performance of the bandstop filter.

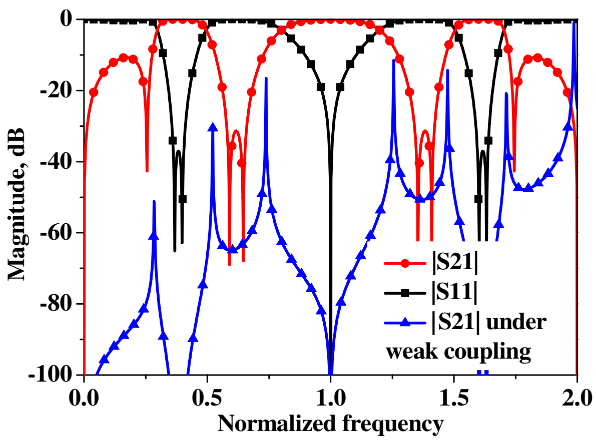

FIGURE 2. Simulated responses of the developed tri-band bandstop filter under weak coupling.

2.2. Transmission Zeros

According to [13], the relationship among S_{21}, Y_{ino}, and Y_{ine} is as follows:

$$S_{21} = \frac{Y_0(Y_{\text{ino}} - Y_{\text{ine}})}{(Y_0 + Y_{\text{ine}})(Y_0 + Y_{\text{ino}})} \tag{9}$$

By substituting Eqs. (1) and (3) into Eq. (9), the following relationship is obtained:

$$\alpha(\tan^2\theta)^3 + \beta(\tan^2\theta)^2 + \gamma\tan^2\theta + \delta = 0 \tag{10}$$

$$\begin{aligned} \alpha =& Z_{o3}Z_sC_eA_o - Z_{e3}Z_sC_oA_e - Z_{e3}Z_{o3}A_eA_o \\ \beta =& Z_{o3}Z_s(D_eA_o - C_eB_o) - Z_{e3}Z_s(D_oA_e - C_oB_e) \\ & - Z_{e3}Z_{o3}(A_eA_o - A_eB_o - A_oB_e) \\ \gamma =& - Z_{o3}Z_sD_eB_o + Z_{e3}Z_sD_oB_e \\ & + Z_{e3}Z_{o3}(A_eB_o + A_oB_e - B_eB_o) \\ \delta =& - Z_{e3}Z_{o3}B_eB_o \end{aligned} \tag{11a}$$

$$\begin{aligned} A_o =& Z_{o3}Z_{o2} + Z_{o3}Z_{o1} + Z_{o2}^2 \\ B_o =& Z_{o2}Z_{o1} \\ C_o =& - Z_{o2}^2 \\ D_o =& Z_{o3}Z_{o2} + Z_{o3}Z_{o1} + Z_{o2}Z_{o1} \end{aligned} \tag{11b}$$

$$\begin{aligned} A_e =& Z_{e3}Z_{e2} + Z_{e3}Z_{e1} + Z_{e2}^2 \\ B_e =& Z_{e2}Z_{e1} \\ C_e =& - Z_{e2}^2 \\ D_e =& Z_{e3}Z_{e2} + Z_{e3}Z_{e1} + Z_{e2}Z_{e1} \end{aligned} \tag{11c}$$

From the above equations, it can be observed that Eq. (10) is a cubic equation in terms of $\tan^2\theta$. Furthermore, via calculation, it can be determined that $\pi/2$ is a solution to the aforementioned equation.

Owing to the considerable complexity of the aforementioned equation, exact closed-form solutions are difficult to obtain. However, given that $\pi/2$ is a known solution, two or four solutions for θ within the DC to $2f_0$ frequency range can be realized by properly tuning the impedance values of the respective sections.

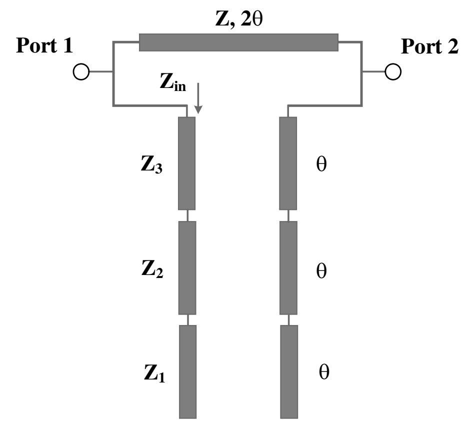

FIGURE 3. Schematic diagram of the triple-band bandstop filter based on non-coupled tri-section stepped-impedance resonators.

2.3. Operating Frequencies

As documented in [14], for parallel coupled lines, the product of even- and odd-mode characteristic impedances (Z_e and Z_o) is equal to the square of the single-line characteristic impedance (Z) when the other line is present, i.e., $Z^2 = Z_eZ_o$. Therefore, for the coupled tri-section stepped-impedance resonators, the structure can be equivalently represented as two independent sets of tri-section stepped-impedance resonators with characteristic impedances given by $Z_1^2 = Z_{e1}Z_{o1}$, $Z_2^2 = Z_{e2}Z_{o2}$, and $Z_3^2 = Z_{e3}Z_{o3}$, which is illustrated in Fig. 3. Accordingly, for the tri-section stepped-impedance resonator in Fig. 3, the input impedance Z_{in} is expressed as:

$$Z_{\text{in}} = jZ_3\frac{(Z_3Z_2 + Z_3Z_1 + Z_2^2)\tan^2\theta - Z_2Z_1}{-Z_2^2\tan^3\theta + (Z_3Z_2 + Z_3Z_1 + Z_2Z_1)\tan\theta} \tag{12}$$

Consequently, by setting $Z_{\text{in}} = 0$, the three operating frequencies can be obtained as follows:

$$\theta_1 = \arctan\sqrt{\frac{1}{K_1K_2 + K_1 + K_2}} \tag{13a}$$

$$\theta_2 = \frac{\pi}{2} \tag{13b}$$

$$\theta_3 = \pi - \theta_1 \tag{13c}$$

where $K_1 = Z_3/Z_2$, $K_2 = Z_2/Z_1$.

In summary, when designing a triple-band bandstop filter using coupled tri-section stepped-impedance resonators, the three stopband frequencies are not independently controllable. Specifically, the center frequency of the second stopband is determined solely by the electrical-length scaling and is independent of the characteristic impedances of the stepped-impedance resonators, whereas the center frequencies of the first and third stopbands are inherently constrained to be symmetric about this center frequency.

2.4. Triple-Band Bandstop Filter Design

Based on the aforementioned analysis and calculations, the center frequency of the second stopband is selected as 3 GHz, while the center frequencies of the first and third stopbands are chosen as 1.2 GHz and 4.8 GHz, respectively. Specifically, since Z_2 is required to be greater than Z_3 yet smaller than Z_1, and since the practical range of microstrip characteristic impedances is generally bounded between $20\,\Omega$ and $130\,\Omega$ to ensure quasi-TEM operation, $Z_2 = 75\,\Omega$ was accordingly selected within this feasible range rather than arbitrarily assigned. Therefore, based on Eq. (13a), with Z_2 preset to $75\,\Omega$ and center frequencies of the first and third stopbands fixed at 1.2 GHz and 4.8 GHz, respectively, the corresponding characteristic impedances are determined as $Z_1 = 110\,\Omega$ and $Z_3 = 53\,\Omega$. Accordingly, $Z_{o1}Z_{e1} = 110^2\,\Omega^2$, $Z_{o2}Z_{e2} = 75^2\,\Omega^2$, and $Z_{o3}Z_{e3} = 53^2\,\Omega^2$ can be established, respectively.

Since the product of even- and odd-mode impedances for each section is fixed, the individual values of Z_e and Z_o cannot be uniquely determined. Therefore, the coupling coefficient of each section, defined as $C = (Z_e - Z_o)/(Z_e + Z_o)$, is set to a constant value of 0.16. In principle, the coupling coefficient of each coupled section is independently adjustable. Nevertheless, it has been observed that independently tuning each coupling coefficient produces essentially the same effect as uniformly adjusting all coupling coefficients. Accordingly, a uniform coupling coefficient C is adopted for all coupled sections in this design.

Consequently, the corresponding even- and odd-mode impedances are obtained as follows: $Z_{e1} = 130\,\Omega$, $Z_{o1} = 94\,\Omega$; $Z_{e2} = 90\,\Omega$, $Z_{o2} = 65\,\Omega$; and $Z_{e3} = 65\,\Omega$, $Z_{o3} = 47\,\Omega$. Simulated responses of the proposed triple-band bandstop filter versus Z_s are plotted in Fig. 4. As illustrated in Fig. 4, as Z_s gradually increases, the return loss in both sides of the stopbands progressively increases; conversely, the return loss between stopbands progressively decreases. Furthermore, the rejection levels within each stopband remain essentially unchanged, whereas the stopband bandwidths gradually broaden with increasing Z_s.

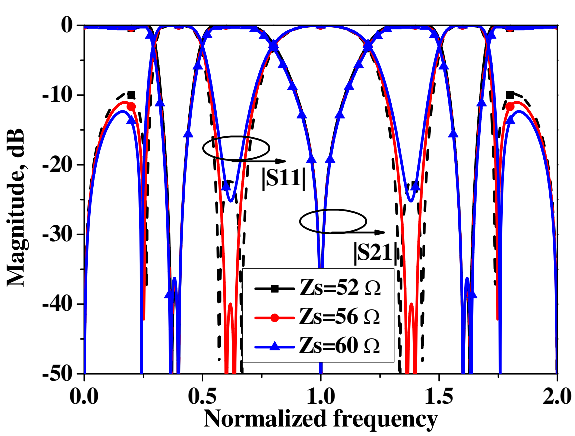

FIGURE 4. Simulated responses of the proposed triple-band bandstop filter versus Z_s. ($Z_{e1} = 130\,\Omega$, $Z_{o1} = 94\,\Omega$, $Z_{e2} = 90\,\Omega$, $Z_{o2} = 65\,\Omega$, $Z_{e3} = 65\,\Omega$, $Z_{o3} = 47\,\Omega$).

To distinguish from the counterpart in Fig. 3, simulated responses of the proposed triple-band bandstop filter and its counterpart are presented in Fig. 5. For the sake of fairness, the return loss at both sides of the stopbands is set to 10 dB for

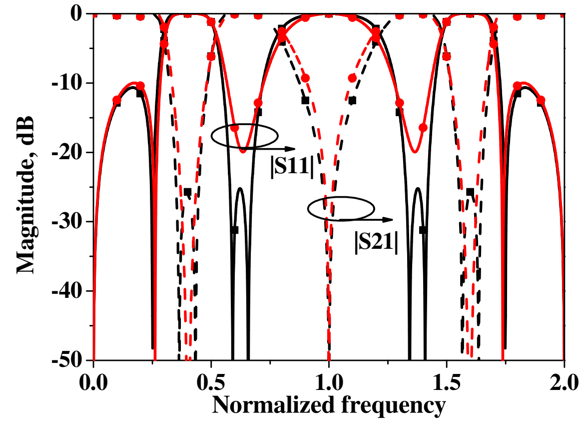

FIGURE 5. Simulated responses of the proposed triple-band bandstop filter (Black lines) in comparison with those of a non-coupled tri-section stepped-impedance resonator-based counterpart (Red lines). ($Z_{e1} = 130\,\Omega$, $Z_{o1} = 94\,\Omega$, $Z_{e2} = 90\,\Omega$, $Z_{o2} = 65\,\Omega$, $Z_{e3} = 65\,\Omega$, $Z_{o3} = 47\,\Omega$, $Z_s = 52\,\Omega$, $Z = 60\,\Omega$).

both configurations. As depicted in Fig. 5, compared with the structure in Fig. 3, the proposed triple-band bandstop filter exhibits significantly larger inter-stopband return loss. Moreover, owing to the employed coupled-resonator topology, the operational bandwidths of all stopbands are substantially wider than those of the conventional structure in Fig. 3.

It is worth noting that the operational bandwidths and rejection levels within the stopbands of the proposed bandstop filter can be flexibly tuned by adjusting the coupling coefficient C between the respective parallel coupled lines. As illustrated in Fig. 6, with Z_s maintained unchanged, both the operational bandwidths of the respective stopbands and the in-band rejection levels are simultaneously affected by the coupling coefficient C. Specifically, as C progressively increases, stopband bandwidths gradually broaden, whereas the corresponding rejection levels within the stopbands conversely diminish.

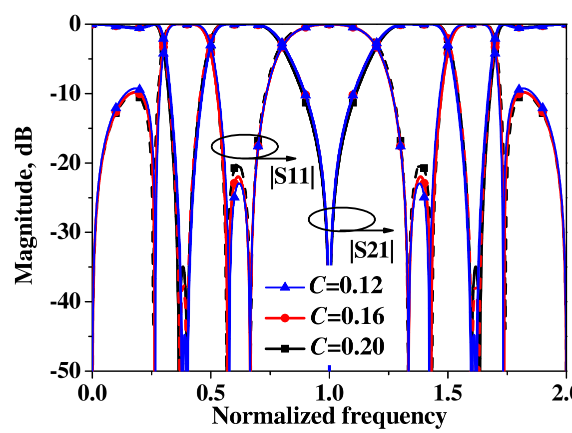

FIGURE 6. Simulated responses of the proposed bandstop filter versus C. ($Z_s = 52\,\Omega$).

3. RESULTS AND DISCUSSION

Based on the preceding analysis and derived equations, center frequencies of the three stopbands are designated as 1.2 GHz, 3 GHz, and 4.8 GHz, respectively, with the maximum out-of-

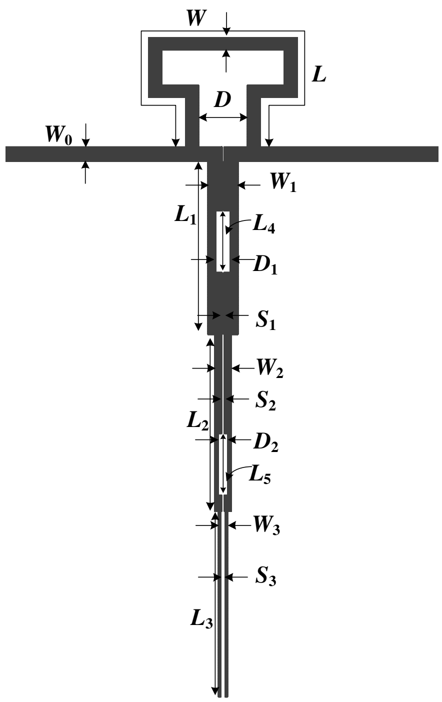

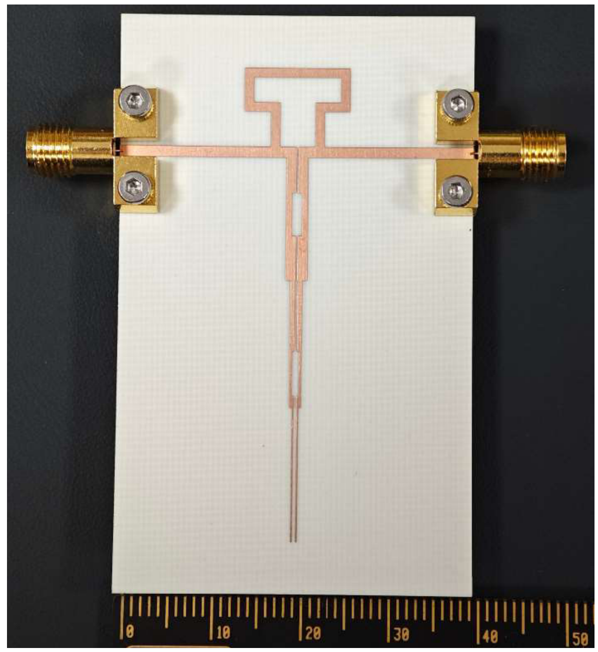

FIGURE 7. Layout and photograph of the developed triple-band bandstop filter. ($W_0 = 1.15\,\text{mm}$, $W = 1.05\,\text{mm}$, $W_1 = 2.4\,\text{mm}$, $W_2 = 1.3\,\text{mm}$, $W_3 = 0.7\,\text{mm}$, $L = 35.7\,\text{mm}$, $L_1 = 14\,\text{mm}$, $L_2 = 14.3\,\text{mm}$, $L_3 = 15\,\text{mm}$, $L_4 = 5\,\text{mm}$, $L_5 = 5\,\text{mm}$, $D = 4\,\text{mm}$, $D_1 = 1.2\,\text{mm}$, $D_2 = 0.8\,\text{mm}$, $S_1 = 0.2\,\text{mm}$, $S_2 = 0.3\,\text{mm}$, $S_3 = 0.4\,\text{mm}$).

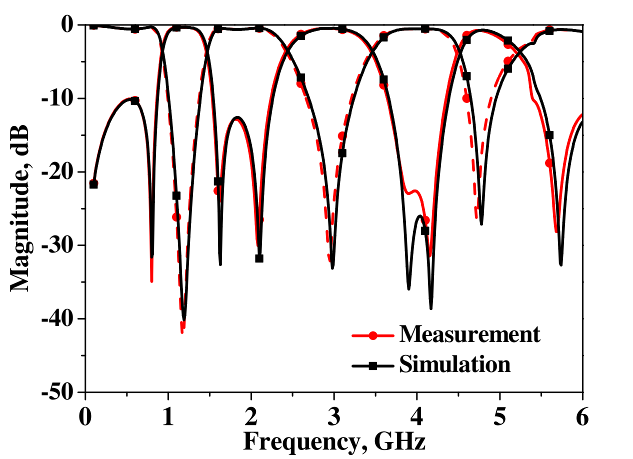

FIGURE 8. Simulated and measured results of the developed triple-band bandstop filter.

band return loss greater than 10 dB. To ensure fabrication feasibility, the coupling coefficient C is selected as 0.16. Consequently, theoretical circuit parameters are determined as follows: $Z_{e1} = 130\,\Omega$, $Z_{o1} = 94\,\Omega$, $Z_{e2} = 90\,\Omega$, $Z_{o2} = 65\,\Omega$, $Z_{e3} = 65\,\Omega$, $Z_{o3} = 47\,\Omega$, and $Z_s = 52\,\Omega$. The Rogers 4003C substrate with a thickness of 20 mil is adopted for implementation. Subsequently, by utilizing the LineCalc tool in Keysight Advanced Design System (ADS), the actual physical dimensions can be readily obtained from theoretical circuit parameters and selected substrate specifications. After fine-tuning, the final optimized parameters are presented in Fig. 7. The design process employed a two-stage simulation approach. Initially, circuit-level preliminary simulation and optimization were performed using Agilent ADS 2020 to obtain ideal electrical parameters and circuit responses. The circuit layout and the photograph of the fabricated prototype are also provided in Fig. 7.

As depicted in Fig. 8, simulated and measured S-parameters of the proposed triple-band bandstop filter are presented. The electromagnetic simulation is performed using the full-wave commercial software Ansys HFSS 2020 R2, whereas the experimental characterization is carried out utilizing the Keysight 5071C vector network analyzer. As observed from this figure, measured results exhibit excellent agreement with simulated predictions. Specifically, the rejection levels within all three stopbands exceed 27 dB. Meanwhile, outside the stopbands, the return loss remains above 10 dB, with a minimum insertion loss of approximately 0.5 dB.

To rigorously demonstrate the performance merits of the proposed triple-band bandstop filter, a comprehensive comparison between the developed design and state-of-the-art counterparts is presented in Table 1, and key performance metrics are systematically evaluated. Based on the analysis of Table 1, the proposed design, which employs a coupled-resonator topology, exhibits superior stopband rejection levels and operational bandwidths compared to previously reported counterparts. Furthermore, the presence of multiple transmission poles within passband regions significantly improves roll-off characteristics at stopband edges. More importantly, a bandstop filter must simultaneously suppress undesired signals in the stopband while preserving the effective transmission of signals outside the stopband; consequently, minimal out-of-band insertion loss and substantial return loss must be carefully considered and

TABLE 1. Comparison with previously reported structures.

Ref.	$f_1/f_2/f_3$ (GHz)	Rejection Level (dB)	Transmission Poles/Zeros	Return Loss*	Layer	Size ($\lambda_g \times \lambda_g$)
[5]	2.4/3.5/5.2	23/27/34	6/3	> 5 dB	Single	0.22×0.1
[6]	2.58/6.88/10.67	30/29/28	4/3	> 10 dB	Single	0.13×0.08
[7]	1.56/2.45/3.46	18/28/35	7/5	> 8 dB	Single	0.16×0.15
[8]	2.57/4.62/7.92	28/26/24	4/3	> 10 dB	Single	0.08×0.08
[9]	1.98/5.6/7.78	29/25/25	3/3	> 5 dB	Single	0.49×0.13
[10]	2.46/3.42/4.08	30/15/18	6/4	> 5 dB	Dual	NA
[11]	2.37/3.54/5.01	31/31/40.5	7/3	> 10 dB	Single	0.6×0.1
This work	**1.2/3/4.8**	**40/32/27**	**8/5**	$\mathbf{-10}$ **dB**	**Single**	$\mathbf{0.35 \times 0.08}$

* The return loss herein refers to that of the passbands out of the stopbands.

rigorously optimized during the design process. Specifically, since the employed resonators are not meandered or folded, the overall circuit size of the proposed filter is comparatively larger than some previously reported compact designs. This trade-off between structural simplicity and size miniaturization has now been explicitly discussed in the revised manuscript.

4. CONCLUSION

In this paper, a triple-band bandstop filter based on coupled tri-section stepped-impedance resonators is proposed. The bandwidths of stopbands as well as the rejection levels within stopband can be flexibly controlled by adjusting the coupling strength between resonators. Furthermore, in the proposed design, minimal out-of-band insertion loss and substantial return loss are simultaneously achieved, thereby ensuring effective signal transmission outside the stopband while maintaining excellent impedance matching.

ACKNOWLEDGEMENT

This work was supported by the National Natural Science Foundation of China under Grant 62201291, the Educational Research Project of the Nantong Vocational and Technical Education Association (Grants NTZJXH2504 and NTZJXH2528), the Natural Science and Technology Project of Jiangsu College of Engineering and Technology (Grant JSGYZRJJZD-03) and the Nantong Natural Science Foundation Project (Grants JCZ2025029 and JC2025042).

REFERENCES

[1] Uchida, H., H. Kamino, K. Totani, N. Yoneda, M. Miyazaki, Y. Konishi, S. Makino, J. Hirokawa, and M. Ando, "Dual-band-rejection filter for distortion reduction in RF transmitters," *IEEE Transactions on Microwave Theory and Techniques*, Vol. 52, No. 11, 2550–2556, Nov. 2004.

[2] Lee, K., J. Lee, and J. Lee, "Wide-passband bandstop filters," *IEEE Microwave Magazine*, Vol. 27, No. 6, 96–104, Jun. 2026.

[3] Sullca, J. F. V., S. Cogollos, V. E. Boria, M. Guglielmi, S. Bastioli, and R. V. Snyder, "Dual-reject-band filters with resonant apertures in rectangular waveguide," *IEEE Transactions on Microwave Theory and Techniques*, Vol. 73, No. 1, 606–619, Jan. 2025.

[4] Hong, J.-S., *Microstrip Filters for RF/Microwave Applications*, 2nd ed., Wiley, Hoboken, NJ, USA, 2011.

[5] Janković, N., R. Geschke, and V. Crnojević-Bengin, "Compact tri-band bandpass and bandstop filters based on Hilbert-fork resonators," *IEEE Microwave and Wireless Components Letters*, Vol. 23, No. 6, 282–284, Jun. 2013.

[6] Dhakal, R. and N.-Y. Kim, "A compact symmetric microstrip filter based on a rectangular meandered-line stepped impedance resonator with a triple-band bandstop response," *The Scientific World Journal*, Vol. 2013, No. 1, 457693, 2013.

[7] Ai, J., Y. H. Zhang, K. D. Xu, M. K. Shen, and W. T. Joines, "Miniaturized frequency controllable band-stop filter using coupled-line stub-loaded shorted SIR for tri-band application," *IEEE Microwave and Wireless Components Letters*, Vol. 27, No. 7, 627–629, Jul. 2017.

[8] Koirala, G. R. and N.-Y. Kim, "Compact and tunable microstrip tri-band bandstop filter incorporating open-stubs loaded stepped-impedance-resonator," *Microwave and Optical Technology Letters*, Vol. 59, No. 4, 815–818, Apr. 2017.

[9] Koirala, G. R. and N.-Y. Kim, "Multiband bandstop filter using an I-stub-loaded meandered defected microstrip structure," *Radioengineering*, Vol. 25, No. 1, 61–66, 2016.

[10] Xiao, J.-K. and Y.-F. Zhu, "New U-shaped DGS bandstop filters," *Progress In Electromagnetics Research C*, Vol. 25, 179–191, 2012.

[11] Ning, H., J. Wang, Q. Xiong, and L.-F. Mao, "Design of planar dual and triple narrow-band bandstop filters with independently controlled stopbands and improved spurious response," *Progress In Electromagnetics Research*, Vol. 131, 259–274, 2012.

[12] Tang, W. and J.-S. Hong, "Coupled stepped-impedance-resonator bandstop filter," *IET Microwaves, Antennas & Propagation*, Vol. 4, No. 9, 1283–1289, 2010.

[13] Matthaei, G. L., L. Young, and E. M. T. Jones, *Microwave Filters, Impedance-Matching Networks, and Coupling Structures*, Artech House, Norwood, MA, USA, 1980.

[14] Pozar, D. M., *Microwave Engineering*, 4th ed., Wiley, Hoboken, NJ, USA, 2011.